International Journal of Applied Mechanics
Vol. 8, No. 3 (2016) 1650042 (16 pages)

DOI: 10.1142/S1758825116500423

World Scientific
www.worldscientific.com

Dependence of Thermal Shock Crack on Specimen Width for Ceramic Materials

Xianghong Xu*, Wenjun Yuan† and Cheng Tian‡
State Key Laboratory of Nonlinear Mechanics
Institute of Mechanics
Chinese Academy of Sciences
Beijing 100190, People's Republic of China
**xxh@lnm.imech.ac.cn*
†*yuanwenjun@lnm.imech.ac.cn*
‡*tiancheng@imech.ac.cn*

Received 24 February 2016
Revised 4 March 2016
Accepted 5 March 2016
Published 22 April 2016

Knowledge of size effect of thermal shock properties of ceramics is a prerequisite in engineering applications. In the present study, the size effect of the cracking in the ceramic materials subjected to water quenching has been experimentally conducted. Based on the Rizk model, the equivalent specimen width of the elastic strip with cracks is introduced and modified to describe the effect of cracks on the deformation of the elastic strip underwater quenching. It is found that the simulation obtained from the proposed modified model is in good agreement with the experimental results. And the reasons for the size effect of crack depth and crack growth into the compressive region are well analyzed by theoretical results. The proposed model is expected to provide a powerful tool to characterize and predict the size effect on thermal shock crack of ceramic materials.

Keywords: Ceramics; thermal shock; size effect.

1. Introduction

To date, more and more metal alloy parts are replaced by ceramics for their high temperature resistances. However, ceramics exhibit low resistance to fracture by thermal shock due to their brittleness, and often occur in cracking or worse, even a highly catastrophic failure. Many researchers focus on studying the thermal shock properties of ceramics in order to promote the thermal shock resistances for their engineering applications. The results obtained from laboratory experiments often performed on samples with small size, while the engineering components under high

*Corresponding author.

temperature are much larger [Glandus and Boch, 1981]. Therefore, it is important to study the size effect of thermal shock properties of ceramics.

Hasselman [1970] predicted that the residual strength after thermal shock was inversely proportional to the 1/4 power of the rod diameter and this prediction was supported by experimental data. Becher [1980] experimentally studied the effects of specimen size and shape on the critical thermal shock temperature ΔT_c. He found that the specimen size has a significant effect on ΔT_c while the shape is not. Sherman and Schlumm [2000] analyzed the effect of ceramic plate thickness on the driving force for cracking and obtained the relationship between ΔT_c and the thickness which is consistent with that of Becher. Lutz [1995] investigated the size effect on ΔT_c for alumina tubes with different diameters, lengths, and wall thicknesses. He found that the wall thickness has a significant effect on ΔT_c, compared to the relatively weak effects of tube diameter and length. Wu *et al.* [2015] examined the size effect on thermal-shock cracks and found that the crack length of the longest level showed an increasing trend with the increase of the specimen width. She *et al.* [2002] and Ding *et al.* [2006] evaluated the thermal shock behavior of porous silicon carbide (SiC) ceramics as a function of quench temperature, quench cycles, and specimen thickness. It is shown that the residual strength of the quenched specimens decreases gradually with increases in the quench temperature and specimen thickness. Jiang *et al.* [2012] examined the mechanism of formation of thermal shock crack patterns in ceramics by the numerical simulations of the thermal shock crack based on the minimum potential energy principle. Li *et al.* [2013] proposed a non-local failure model to simulate the thermal shock crack evolution. By using this numerical model, the initiation and propagation of cracks in water quenched ceramic specimens were simulated. Bourdin *et al.* [2014] used a quasi-static gradient damage model to study the genesis and selective propagation of complex crack networks induced by thermal shock showing that the propagation of fully developed cracks follows Griffith criterion and depends only on the fracture toughness, while crack morphogenesis is driven by the material's internal length. Lammi *et al.* [2015] simulated the dynamic compaction and fracture of concrete at the mesoscale, and fracture within bulk phases and along interfaces in the structures is modeled using the cohesive finite element method.

In this study, experiments were conducted on the thermal shock cracks, as well as a quantitative characterization approach of the depth and spacing of the long crack in the experiment were carried out to investigate the size effect on thermal shock crack of ceramic materials. In the profile of the theoretical analysis, the equivalent specimen width of the elastic strip with cracks is introduced and modified to describe the effect of cracks on the deformation of the elastic strip under thermal shock. The crack depth can be further obtained with the Griffith crack propagation criterion and compared with the experimental results. According to the simulation results, the reasons for the size effect of crack

depth and crack growth into the compressive region have been investigated and analyzed.

2. Experimental Details and Results

Commercially available Al_2O_3 powder (particle size 0.5 μm, purity 99.5%) was compressed into blocks at 20 MPa and subsequently sintered at 1650℃ for 2 h at normal pressure. The sintered bodies with 4% porosity and 10 μm mean grain size, were cut into specimens with dimensions of 50 mm × 5 mm × $2H$, the specimen width $2H$ = 1.5, 2.5, 5, 7.5, 10, 15, 20, 25, 30, 40 and 50 mm, as show in Fig. 1.

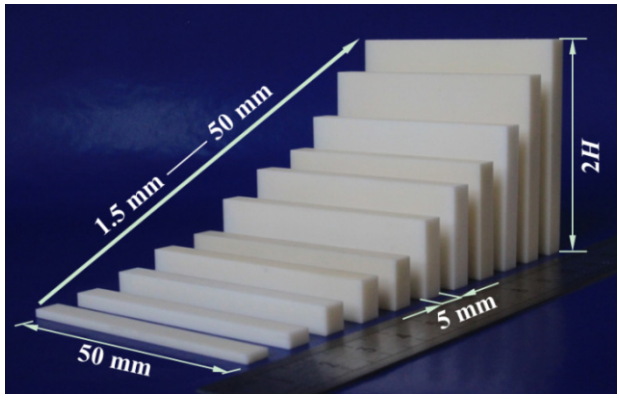

Fig. 1. Ceramic specimen with dimensions of 50 mm × 5 mm × $2H$. The specimen width $2H$ ranged from 1.5 mm to 50 mm.

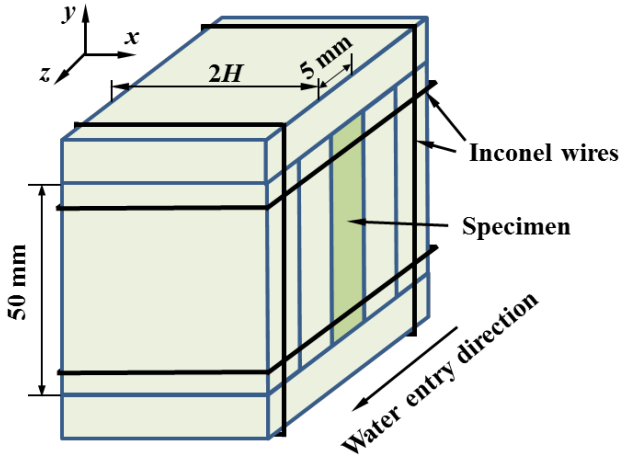

Fig. 2. Stack of specimen prepared for thermal shock test. Arrows indicated the water entry direction, the cooled and interior surfaces of the specimen, respectively.

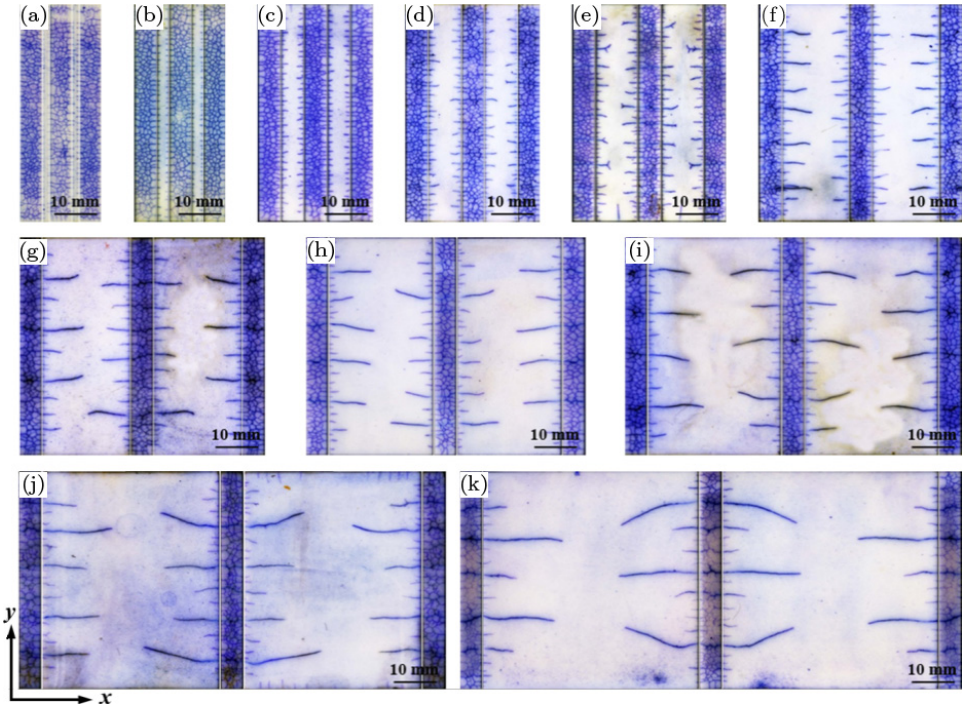

Fig. 3. Thermal shock cracks on interior surface ($50\,\text{mm} \times 2H$) and cooled surface ($50\,\text{mm} \times 10\,\text{mm}$) of the stacked specimen. The thermal shock temperature and water temperature are 300℃ and 17℃, respectively. The specimen width $2H$ is: (a) 1.5, (b) 2.5, (c) 5, (d) 7.5, (e) 10, (f) 15, (g) 20, (h) 25, (i) 30, (j) 40 and (k) 50 mm.

The specimens were ground, polished, slightly chamfered, and then stacked to prevent coolant from accessing the interior surfaces (Fig. 2). The stacks were initially heated to a pre-determined temperature 300℃ for 20 min in a muffle furnace before quenched in water at 17℃. After drying, the quenched specimen was immersed in dye and then wiped with absorbent cotton. The crack patterns of each specimen after quenching were thus distinguishable and were photographed by a digital scanner (Fig. 3).

Crack depth was defined as the maximum vertical distance from the tip of a crack to the side and its dimensionless expression was obtained by dividing by half the specimen width (H). The statistical distributions of the crack depths versus specimen width are shown in Fig. 4. Furthermore, using the group average method [Sokal and Michener, 1958], the cracks with length grading structure can be divided into long cracks and short cracks. Crack with depths greater and lesser than 0.36 were defined as the long and short cracks, respectively. The absolute value of the long crack depth (solid squares), long crack spacing (hollow squares), and short crack depth (solid triangles) increases linearly with the specimen width (Fig. 5). The dimensionless values of the long crack depths, which

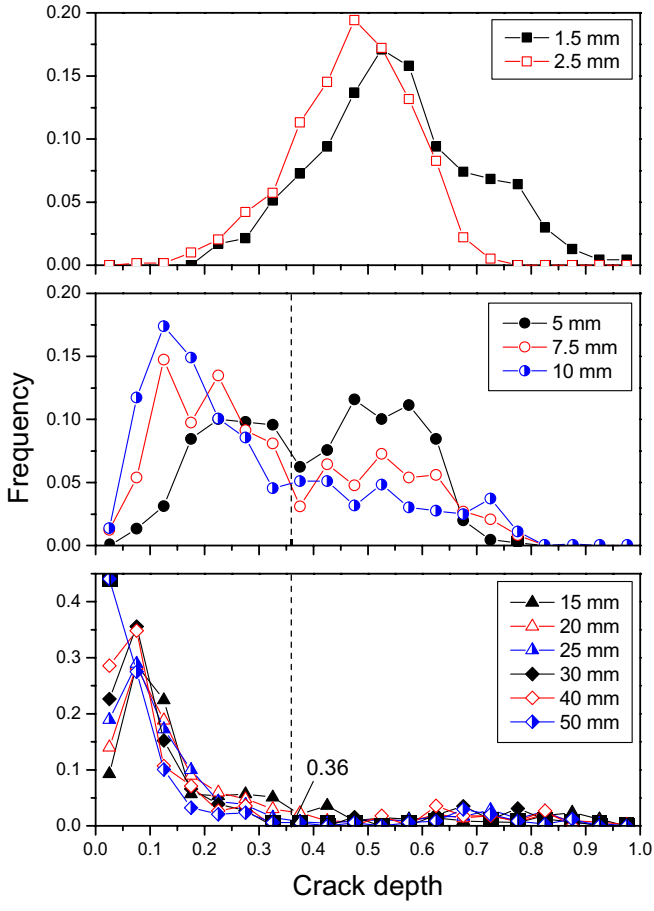

Fig. 4. Statistical distribution of the thermal shock crack depth.

play a major role on the residual strength of shocked specimen, are mainly concerned here (solid diamonds in Fig. 6). Five specimens were selected to measure and analyze the crack characteristics to avoid the occasional cases at each point.

As the specimen width increases, the crack depth evolves from uniform as $2H < 5\,\text{mm}$ to length grading as $2H \geq 5\,\text{mm}$, that is, it turns from the unimodal to a bimodal distribution, and the critical specimen width is 5 mm (Figs. 3 and 4). The absolute values of the long crack depth increase approximately linearly with increasing $2H$ (solid squares and the corresponding line in Fig. 5), while the dimensionless crack depth decreases first and then increases gradually with the same critical specimen width 5 mm, which is mainly caused by length grading (solid diamonds in Fig. 6).

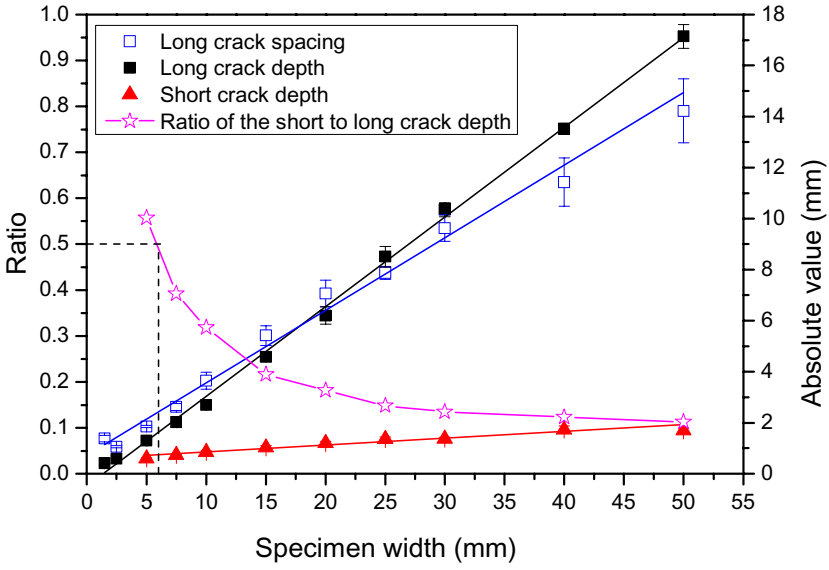

Fig. 5. Absolute values of the crack characterization parameters versus specimen width. Solid squares (■) show the long crack depth, hollow squares (□) show the long crack spacing, solid triangles (▲) show the short crack depth, and hollow pentagrams (☆) show the ratio of the short to long crack depth.

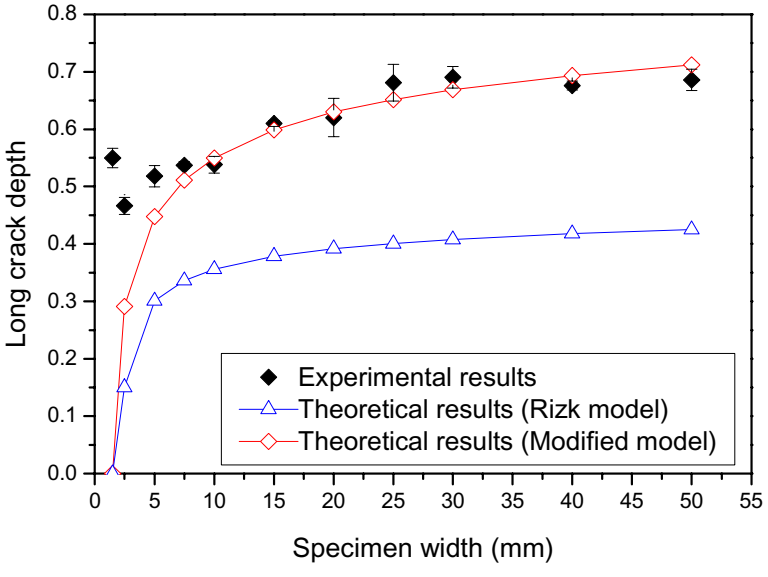

Fig. 6. Long crack depth versus specimen width. Solid diamonds (♦) show the dimensionless values of the experimental results, hollow triangles (△) and diamonds (◇) show the theoretical results obtained from Rizk and our model with $k_c = 0.4$, respectively.

3. Theoretical Model and Analysis

A theoretical model is introduced to depict the above water quenching test. For simplicity, consider a plane stress problem for a homogeneous elastic infinite strip of width $2H$ with parallel periodic cracks of depth b and spacing $2c$ along the surfaces $x = 0$ and $x = 2H$ perpendicular to the boundaries (Fig. 7). Moreover, short crack, whose depth is less than one half of the long crack depth as $2H \geq 7.5\,\text{mm}$ (hollow pentagram in Fig. 5), is not introduced here since the short crack has little effect on the stress intensity factor of the long crack and the residual strength of the specimen. At $t = 0$, the initial temperature of the strip is T_0,

$$T(x,t) = T_0, \quad (t = 0,\ 0 \leq x \leq 2H,\ -\infty < y < +\infty). \tag{1}$$

The strip is quenched on the cracked surfaces in water at T_∞, and can be expressed by the convection boundary condition,

$$\mp k\frac{\partial T}{\partial x} = h[T_\infty - T(x,t)], \quad (t > 0,\ x = 0,\ 2H), \tag{2a}$$

where k is the thermal conductivity, h is the surface heat transfer coefficient. Considering the symmetry of the structure and boundary conditions, the temperature field $T(x,\ y)$ is symmetrical with respect to the plane $x = H$,

$$\frac{\partial T}{\partial x} = 0, \quad (t > 0, x = H, -\infty < y < +\infty). \tag{2b}$$

The thermal stress field of this problem can be solved by the superposition technique introduced by Rizk [2006]. First, the stress field $\sigma^T_{yy}(x,y)$ is obtained from the un-cracked strip. Second, the stress field $\sigma_{yy}(x,y)$ of the isothermal plane cracked

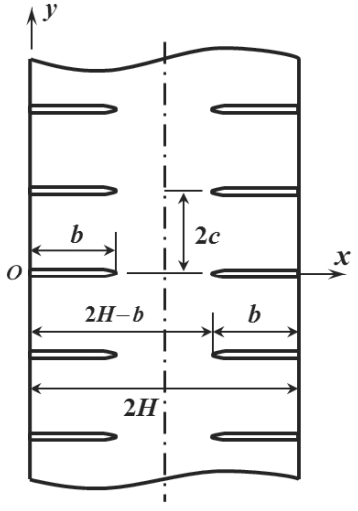

Fig. 7. Geometric model of ceramic sheet with periodic parallel cracks with equal depth and spacing. b is the crack depth, $2c$ is the spacing between cracks, and $2H$ is specimen width.

problem is obtained by applying the negative of stress $-\sigma_{yy}^{T}(x,y)$ on the crack surface. The final stress field can be obtained by the superposition of the $\sigma_{yy}^{T}(x,y)$ and $\sigma_{yy}(x,y)$. Assume that the effect of $\sigma_{yy}^{T}(x,y)$ on the singularity of crack tip is neglected, the stress intensity factor can be obtained by $\sigma_{yy}(x,y)$ or the displacement on the crack face, $v(x,0)$, corresponding to $\sigma_{yy}(x,y)$.

The temperature field $T(x,t)$ of the un-cracked strip satisfies the Fourier heat equation as follows [Ozisik, 1980],

$$\frac{\partial^2 T}{\partial x^2} = \frac{1}{a}\frac{\partial T}{\partial t}, \quad (t > 0, 0 < x < 2H, -\infty < y < +\infty), \tag{3}$$

where a is the thermal diffusivity. According to the initial and boundary condition, Eqs. (1), (2a) and (2b), the temperature field by means of Eq. (3) can be expressed by Ozisik [1980],

$$\frac{T(x,\tau) - T_0}{T_\infty - T_0} = 1 - 2\sum_{n=1}^{\infty} \exp(-\beta_n^2 \cdot \tau) \cdot \frac{\sin\beta_n \cos(\beta_n \cdot x^*)}{\beta_n + \sin\beta_n \cos\beta_n}, \tag{4}$$

where $x^* = 1 - x/H$ is the non-dimensional coordinate, $\tau = ta/H^2$ is the non-dimensional time, $\beta_n (n = 1, 2, \ldots, \propto)$ are the roots of the equation $\beta_n \tan\beta_n = Bi$, and $Bi = kH/h$ is the Biot number. The longitudinal stress $\sigma_{yy}^{T}(x,y)$, that mainly caused the growth of the parallel cracks along x axis, can be expressed by Boley and Weiner [1960],

$$\sigma_{yy}^{T}(x,t) = \alpha E \left\{ -(T - T_0) + \frac{1}{H}\int_0^H (T - T_0)\mathrm{d}x \right\}, \tag{5}$$

where α is the thermal expansion coefficient, E is the elastic modulus. Substitute Eq. (4) with Eq. (5), the stress field of un-cracked body can be deduced by,

$$\frac{\sigma_{yy}^{T}(x^*,\tau)}{\alpha E T_0} = \frac{T_\infty - T_0}{T_0}\left\{ \sum_{n=1}^{\infty} \frac{2\sin\beta_n}{\sin\beta_n\cos\beta_n + \beta_n} \cdot \mathrm{e}^{-\tau\beta_n^2} \left(\cos\beta_n x^* - \frac{\sin\beta_n}{\beta_n} \right) \right\}. \tag{6}$$

The stress field $\sigma_{yy}(x,y)$ of the isothermal plane cracked problem can be obtained by solving the following equilibrium equations:

$$\begin{aligned} (\kappa - 1)\nabla^2 u + 2\left(\frac{\partial^2 u}{\partial x^2} + \frac{\partial^2 v}{\partial x \partial y} \right) = 0, \\ (\kappa - 1)\nabla^2 v + 2\left(\frac{\partial^2 u}{\partial x \partial y} + \frac{\partial^2 v}{\partial y^2} \right) = 0, \end{aligned} \tag{7}$$

where $\kappa = (3 - \mu)/(1 + \mu)$ for plane stress, μ is the Poisson's ratio, and u, v are the x and y components of the displacement vector, respectively. Since $x = H$ is the plane of symmetry and the crack is periodic, it is sufficient to consider the local perturbation problem, $0 < x < H$ and $0 < y < c$. The symmetry boundary

condition at $x = H$ and $y = c$ can be expressed by,

$$u(H, y) = 0, \quad \sigma_{xy}(H, y) = 0, \quad 0 < y < c, \tag{8a}$$

$$v(x, c) = 0, \quad \sigma_{xy}(x, c) = 0, \quad 0 < x < H, \tag{8b}$$

where σ_{xy} is the shear stress. The free boundary conditions at $x = 0$ may be stated as,

$$\sigma_{xx}(0, y) = 0, \quad \sigma_{xy}(0, y) = 0, \quad 0 < y < c, \tag{8c}$$

where σ_{xx} is the x direction stress. Applying the negative of stress, $-\sigma^T_{yy}(x, y)$, on the crack surface, the symmetry boundary conditions at the crack front may be written as,

$$\sigma_{xy}(x, 0) = 0, \quad v(x, 0) = 0, \quad b < x < H, \tag{8d}$$

$$\sigma_{xy}(x, 0) = 0, \quad \sigma_{yy}(x, 0) = -\sigma^T_{yy}(x, y), \quad 0 < x < b, \tag{8e}$$

where σ_{yy} is the y direction stress. Applying the condition Eqs. (8a)–(8e), the partial differential equation Eq. (7) can be reduced to the following integral equation by defining a new function $\varphi(x) = v(x, 0)$,

$$\lim_{y\to 0} \int_0^b [K_1(x, y, s) + K_2(x, y, s)]\varphi(s)\mathrm{d}s = -\frac{\pi(\kappa + 1)}{4G}\sigma^T_{yy}(x, t), \tag{9}$$

where

$$K_1(x, y, s) = \int_0^\infty \left\{ \frac{[(1 - y\gamma)\mathrm{e}^{-4c\gamma} + (y\gamma - 2c\gamma - 1)\mathrm{e}^{-2c\gamma}]\mathrm{e}^{y\gamma}}{(1 - \mathrm{e}^{-2c\gamma})^2} - \frac{[(1 + y\gamma) + (2c\gamma - y\gamma - 1)\mathrm{e}^{-2c\gamma}]\mathrm{e}^{-y\gamma}}{(1 - \mathrm{e}^{-2c\gamma})^2} \right\} \gamma \cos(s - x)\gamma d\gamma, \tag{10}$$

$$K_2(x, y, s) = \frac{\pi}{c} \sum_{n=1}^{\infty} \{I + II\} \cos \alpha_n y,$$

$$\begin{aligned} \mathrm{I} = \frac{1}{2M} \Big\{ & [6\alpha_n - 2\alpha_n^2(2H - x - s)]\mathrm{e}^{(s+x-2H)\alpha_n} \\ & + [10\alpha_n - 6\alpha_n^2(2H - x + s) + 4\alpha_n^3 s(2H - x)]\mathrm{e}^{-(s-x+2H)\alpha_n} \\ & + [10\alpha_n + 6\alpha_n^2(x + s) + 4\alpha_n^3 sx]\mathrm{e}^{(s+x-4H)\alpha_n} \\ & + [6\alpha_n - 2\alpha_n^2(s - x)]\mathrm{e}^{-(s-x+4H)\alpha_n} \Big\}, \end{aligned} \tag{11}$$

$$\begin{aligned} \mathrm{II} = \frac{1}{2M} \Big\{ & [10\alpha_n - 6\alpha_n^2(x + s) + 4\alpha_n^3 sx]\mathrm{e}^{-(s+x)\alpha_n} \\ & + [10\alpha_n - 6\alpha_n^2(2H + x - s) + 4\alpha_n^3 x(2H - s)]\mathrm{e}^{(s-x-2H)\alpha_n} \end{aligned}$$

$$+[6\alpha_n+2\alpha_n^2(2H-x-s)]\mathrm{e}^{-(s+x+2H)\alpha_n}$$
$$+[6\alpha_n+2\alpha_n^2(s-x)]\mathrm{e}^{(s-x-4H)\alpha_n}\Big\},$$
$$M=1+4\alpha_n H\mathrm{e}^{-2\alpha_n H}-\mathrm{e}^{-4\alpha_n H},$$

where $\sigma_n = n\pi/c$. The numerical integration technique developed by Kaya and Erdogan [1986a, b] is employed to solve Eq. (9) and carry out $\varphi(x)$. And then the stress intensity factors of the periodic parallel straight cracks can be expressed by,

$$K_{\mathrm{I}}(b)=\frac{2\sqrt{2\pi}G}{\kappa+1}\lim_{x\to b}\frac{v(x,0)}{\sqrt{b-x}}=\frac{2\sqrt{2\pi}G}{\kappa+1}\lim_{x\to b}\frac{\varphi(x)}{\sqrt{b-x}}, \tag{12}$$

where G is the shear modulus.

The schematic of the deformation of the elastic strip with cracks under the thermal shock is shown in Fig. 8. The strip at preset temperature T_0 is shown in Fig. 8(a), taking the part ranges from $y = 0$ to $y = c$ as the research object. The temperature field $T(x, t)$ of the strip changes as it is subjected to water quenching, and the deformation of the research object without cracks is $\triangle l$ (Fig. 8(b)),

$$\Delta l=\frac{\alpha c}{H}\int_0^H[T(x,t)-T_0]\mathrm{d}x. \tag{13}$$

Underwater quenching, cracks are initiated at the boundary of the specimen. According to the boundary conditions in Rizk, the displacement boundary condition

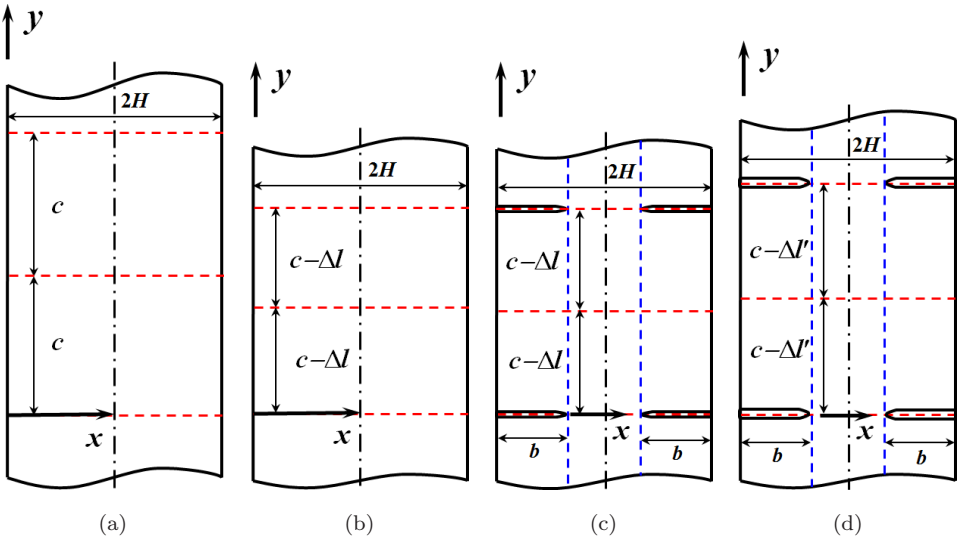

Fig. 8. Schematic of the deformation of the elastic strip with cracks under the water quenching. (a) Research object with length of c taken from the infinite strip; (b) Deformation of the thermal shocked research object without cracks is $\triangle l$; (c) Deformation of the thermal shocked research object with cracks obtained from Rizk model is still $\triangle l$; (d) Actual deformation of the research object with cracks is $\triangle l' < \triangle l$ since the constraint released due to cracks.

$v = 0$ applied at $y = 0$ and $y = c$ (Eqs. (8d) and (8b)). That is, the displacement in the y-direction of crack body at $y = 0$ and $y = c$ equals that of un-cracked body (Fig. 8(c)), and the deformation of the research object with cracks equals Eq. (13).

In fact, the constraint of the crack surface is released due to the generation of the cracks under water quenching. For the research object, the temperature of its lateral part, the domain of $0 < x < b$ and $2H - b < x < 2H$, is lower than that of the central part, the domain of $b \leq x \leq 2H - b$. The two parts are mutually restraint and have the same deformation before cracking, while the constraint of the lateral part on the central part is greatly decreased after cracking. Therefore, the deformation of the research object with crack, which is dominated by the central part, is less than $\triangle l$ and defined as $\triangle l'$ shown in Fig. 8(d). However, the constraint relaxation due to crack is not taken into account in the above model.

Assume that the deformation of the research object $\triangle l'$ satisfies (Fig. 8(d)),

$$\Delta l' = \frac{\alpha c}{q} \int_{H-q}^{H} [T(x,t) - T_0] \mathrm{d}x, \tag{14}$$

where $q = H - b\mathrm{e}^{-k_c \cdot c/H}$ is the equivalent specimen width of the research object with cracks, the equivalent coefficient $k_c > 0$ is a parameter to describe the effect of cracks on the deformation of research object, and which k_c is smaller, the effect is greater. In the case of $k_c \to \infty$, there is $q = H$ and $\triangle l' = \triangle l$, the effect of the lateral part on the central part is almost the same as that of no cracks body, and Eq. (14) can be deduced to Eq. (13) which is corresponding to Rizk model. In the case of $k_c \to 0$, the lateral part almost has no constraint on the deformation of the central part, the deformation of the research object is determined by the central part, and there is $q = H - b$ and

$$\Delta l' = \frac{\alpha c}{H - b} \int_{b}^{H} [T(x,t) - T_0] \mathrm{d}x, \tag{15}$$

In order to make the research object have the deformation as shown in Fig. 8(d), the deformation of $\Delta l'$ (Fig. 8(d)) is applied to the quenched un-cracked body (Fig. 8(b)), that is, the boundary condition at $y = 0$ and $y = c$ can be expressed by $v = 0$ and $v = \triangle l - \triangle l'$, respectively. The stress field can be expressed by,

$$\begin{aligned} \sigma'^{T}_{yy}(x,t) &= \alpha E \left\{ -(T - T_0) + \frac{1}{q} \int_{H-q}^{H} (T - T_0) \mathrm{d}x \right\} \\ &= \alpha E (T_\infty - T_0) \left\{ \sum_{n=1}^{\infty} \frac{2 \sin \beta_n}{\sin \beta_n \cos \beta_n + \beta_n} \cdot \mathrm{e}^{-\tau \beta_n^2} \left(\cos \beta_n x^* - \frac{H \sin(\beta_n q/H)}{q \beta_n} \right) \right\}. \end{aligned} \tag{16}$$

The boundary condition Eq. (9) can be rewritten as follows:

$$\lim_{y \to 0} \int_0^b [K_1(x,y,s) + K_2(x,y,s)] \varphi(s) \mathrm{d}s = -\frac{\pi(\kappa + 1)}{4G} \sigma'^{T}_{yy}(x,t). \tag{17}$$

The modified stress intensity factor can be obtained by substitute $\varphi(x)$ obtained from Eq. (17) to Eq. (12).

4. Results and Discussion

In the present calculation, the initial temperature of the specimen $T_0 = 300°\mathrm{C}$, the water temperature $T_\infty = 17°\mathrm{C}$, and the thermal expansion coefficient $\alpha = 6.8 \times 10^{-6}\,\mathrm{K}^{-1}$, thermal conductivity $k = 31\,\mathrm{W/(m \cdot K)}$, constant-pressure specific heat is denoted by c, density is denoted by ρ, elastic modulus $E = 370\,\mathrm{GPa}$, the heat transfer coefficient $h = 50\,\mathrm{kW/(m^2 \cdot K)}$, Poisson's ratio $\mu = 0.22$ [Zhang and Ma, 2006]. $K_{\mathrm{IC}} = 123.5\,\mathrm{MPa \cdot mm^{1/2}}$ where the strain energy release rate is taken as $42.5\,\mathrm{J \cdot m^{-2}}$ [Bourdin *et al.*, 2014]). The long crack spacing under different specimen width is obtained from our experiments (Hollow squares in Fig. 5).

According to the method introduced by Bahr *et al.* [1988], the terminated crack depth of the above model with different specimen width can be obtained (Fig. 6). At $t = t_1$, the displacement on the crack surface along y-axis $\varphi(x)$ according to Rizk model and the proposed modified model could be calculated by solving Eqs. (9) and (17), respectively, while the crack depth b is a given constant. Meanwhile, the stress intensity factor K_{I} could also be determined by Eq. (12). Therefore, the relationship between K_{I} and b is revealed at t_1, and the envelop curve would be obtained if K_{I} as a function of b at different t_1 is plotted. The terminated crack depth is determined by the cross-point of the critical value K_{IC} horizontal line and the envelope curve. Obviously, there is a big difference between the crack depths obtained from Rizk theoretical model (hollow triangles in Fig. 6) and the experimental results (solid diamonds in Fig. 6). It is found that the values obtained from the proposed modified model are in good agreement with the experimental results as the specimen width $2H \geq 7.5\,\mathrm{mm}$ (Hollow diamonds in Fig. 6), and the equivalent coefficient $k_c = 0.4$.

In the theoretical analysis, the Biot number is increased in parallel with the specimen width $2H$, resulting in the thermal stresses, in Eqs. (6) and (16) respectively for Rizk and the modified models, and stress intensity factor in Eq. (12) both increased, and this will cause the crack to extend further. Meanwhile, the experimental results reveal that the crack spacing $2c$ is increased linearly with an increase in the $2H$. The increase of the equivalent specimen width q and stress in Eq. (16) both result from the crack spacing $2c$, resulting into the terminated crack depth increased. The difference between the values of Rizk and our models, represented by hollow triangles and diamonds in Fig. 6 respectively, indicated the effect of crack spacing on the crack depth due to the increase of specimen width. Furthermore, it should be noted that there are interactions among the cracks while the crack interaction has locality. That is, the interaction becomes slight with an increase in the crack spacing, resulting in a further crack growth.

However, as $2H < 7.5\,\mathrm{mm}$, the crack depth obtained from the proposed modified model shows big difference from the experimental results, and the difference increases with decreasing specimen width (Fig. 6). This indicated that the model is not applicable for small specimen width which is mainly due to the invalid assumption of plane stress and the unstable crack propagation. Finite element is adopted

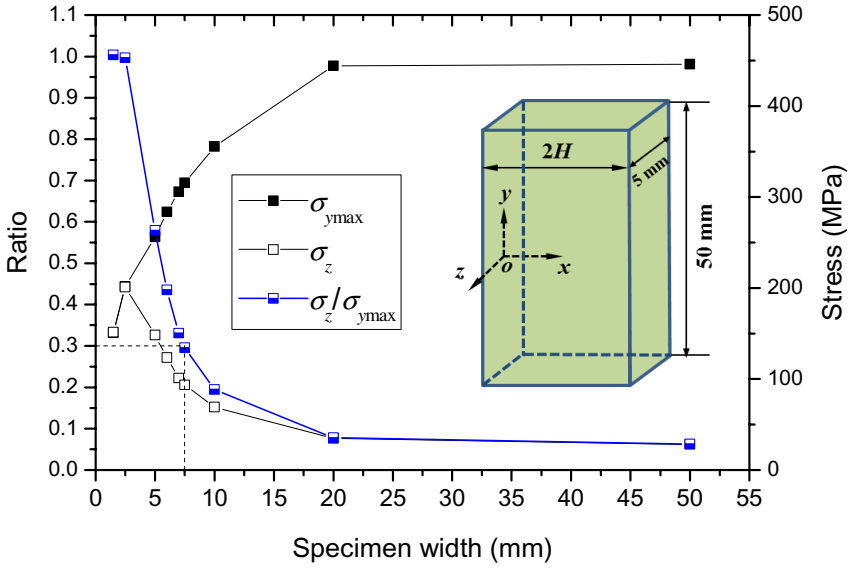

Fig. 9. Thermal stresses ratio $\sigma_z/\sigma_{y\,\max}$ versus specimen width. $\sigma_{y\,\max}$ is the maximum thermal stress in y direction and σ_z is the corresponding thermal stress in z direction. Finite element model with dimensions of $50\,\text{mm} \times 5\,\text{mm} \times 2H$. The origin is located at center of rectangular $50\,\text{mm} \times 5\,\text{mm}$. The specimen is quenched on the surfaces $x = 0$ and $x = 2H$ by convection boundary condition, while other surfaces are insulated. The quench and water temperatures are 300°C and 17°C, respectively.

to calculate the maximum thermal stress in y directions, σ_y, and the corresponding stress in z direction, σ_z, at point O of the specimen with different width $2H$ under the above water quenching test by assuming crack is not generated during the whole process (Fig. 9). Numerical simulations show that during the whole process of water quenching, as the specimen width ranged from 1.5 mm to 50 mm, the stress in the y direction is vital to the crack initiation since the stress in the z direction has been in a low value and has not reached the strength of the ceramic. Therefore, the ratio of $\sigma_z/\sigma_{y\,\max}$ is chosen to analyze the application condition of the plane stress assumption. It can be seen that when the ratio $\sigma_z/\sigma_{y\,\max}$ is larger than 30% as $2H < 7.5\,\text{mm}$, it indicated that σ_z should not be ignored compared to $\sigma_{y\,\max}$ and the assumption of plane stress is no longer valid.

Further, the zero thermal stress position is theoretically analyzed comparative with the terminated crack tip obtained from experiments (Fig. 10). The terminated crack tip, greater than 0.53 (solid diamonds in Fig. 10), obtained from experiments locates between the zero thermal stress positions obtained from Rizk model Eq. (6) (hollow triangles in Fig. 10) and the proposed modified model Eq. (16) (hollow squares in Fig. 10). It is found that the zero thermal stress point obtained from Rizk model does not change along with the specimen size, while that of the proposed modified model changed. This is mainly because the stress field, Eq. (16), obtained from the proposed modified model is dependent on the equivalent specimen width.

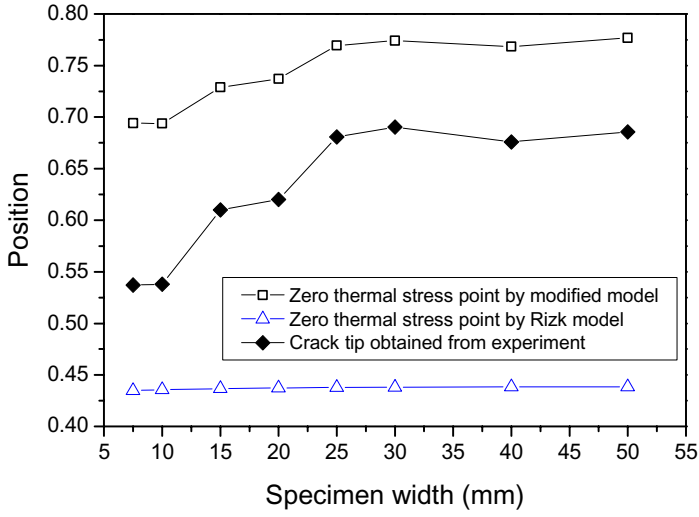

Fig. 10. Positions of the crack tip and zero thermal stress as functions of specimen width. Solid diamonds (♦) show the positions of the terminated crack tip by experiments, hollow triangles (△) and hollow squares (□) show the zero thermal stress positions of Rizk model and our model with $k_c = 0.4$, respectively.

Obviously, the cracks have propagated into the compressive zone predicted by Rizk model. According to the Griffith criterion, the crack may propagate forward only when the stress intensity factor is greater than the critical stress intensity factor, and the stress intensity factor will decrease rapidly to zero as the crack propagates into the compressive zone. In fact, crack is very difficult to propagate into the compressive zone, and the zero thermal stress point predicted by Rizk model is not appropriate in such case and should be modified by the proposed model.

5. Conclusion

In our work, a series of experimental and theoretical works has been done to study the effect of specimen size on the long crack depth, which plays a critical role in determines the residual strength of the ceramic specimen after thermal shock. Experimental results showed that crack depths of the ceramic sheets are almost uniform with a smaller specimen size at a quench temperature of 300℃, they present length grading with a bigger specimen size. The absolute values of the long crack depth and spacing both increase approximately linearly with an increase in the specimen width, while the dimensionless crack depth initially decreases and then increases resulting from length grading in cracks.

Furthermore, a quantitative mode modified from Rizk model has been proposed for the effect of cracks on the deformation of the elastic strip under thermal shock, in which the equivalent specimen width is introduced. It is found that the simulation obtained from the proposed modified model is in good agreement with

the experimental results as the specimen width $2H \geq 7.5\,\text{mm}$. A large difference between the simulation and the experimental results is mainly contributed to the assumption of plane stress adopted in the model. The proposed model has been demonstrated and is expected to provide a powerful tool to characterize and predict size effect on thermal shock crack of ceramic materials.

Acknowledgments

The authors are grateful for the support from the National Natural Science Foundation of China through grant number 11272313.

References

Bahr, H. A., Weiss, H. J., Maschke, H. G. and Meissner, F. [1988] "Multiple crack propagation in a strip caused by thermal shock," *Theoretical and Applied Fracture Mechanics* **10**, 219–226.

Becher, P. F. [1980] "Thermal shock resistance of ceramics. Size and geometry effects in quench tests," *American Ceramic Society Bulletin* **59**, 542.

Boley, B. A. and Weiner, J. H. [1960] *Theory of Thermal Stresses* (John Wiley and Sons, New Jersey), pp. 307–345.

Bourdin, B., Marigo, J.-J., Maurini, C. and Sicsic, P. [2014] "Morphogenesis and propagation of complex cracks induced by thermal shocks," *Physical Review Letters* **112**, 014301.

Ding, S. Q., Zeng, Y. P. and Jiang, D. L. [2006] "Thermal shock resistance of in situ reaction bonded porous silicon carbide ceramics," *Materials Science and Engineering: A* **425**, 326–329.

Glandus, J. C. and Boch, P. [1981] "Influence of the size factor on the thermal shock resistance of ceramic samples," *International Journal of Thermophysics* **2**, 89–101.

Hasselman, D. P. H. [1970] "Strength behavior of polycrystalline alumina subjected to thermal shock," *Journal of the American Ceramic Society* **53**, 490–495.

Jiang C. P. *et al.* [2012] "A study of the mechanism of formation and numerical simulations of crack patterns in ceramics subjected to thermal shock," *Acta Materialia* **60**(11), 4540–4550.

Kaya, A. C., Erdogan, F. [1986a] "On the solution of integral equations with a generalized cauchy kernal," *Quarterly of Applied Mathematics XLV* **45**(3), 455–469.

Kaya, A. C. and Erdogan, F. [1986b] "On the solution of integral equations with strongly singular kernels," *Quarterly of Applied Mathematics XLV* **45**(1), 105–122.

Lammi C. J., Li H., McDowell D. L. and Zhou M. [2015] "Dynamic Fracture and Dissipation Behaviors of Concrete at the Mesoscale," *International Journal of Applied Mechanics* **07**(03), 1550038.

Li J., Song F. and Jiang C.P. [2013] "Direct numerical simulations on crack formation in ceramic materials under thermal shock by using a non-local fracture model," *Journal of the European Ceramic Society* **33**, 2677–2687.

Lutz, E. H. [1995] "Size sensitivity to thermal shock of plasma-sprayed ceramics and factors affecting the size effect," *Journal of the American Ceramic Society* **78**, 2700–2704.

Ozisik, M. N. [1980] *Heat Conduction* (John Wiley & Sons, Inc: New York).

Rizk, A. E.-F. A. [2006] "An elastic strip with periodic surface cracks under thermal shock," *International Journal of Engineering Science* **44**, 807–818.

She J. H., Ohji, T. and Deng, Z. Y. [2002] "Thermal shock behavior of porous silicon carbide ceramics," *Journal of the American Ceramic Society* **85**(8), 2125–2127.

Sherman, D. and Schlumm, D. [2000] "Thickness effect in thermal shock of alumina ceramics," *Scripta Materialia* **42**, 819–825.

Sokal, R. and Michener, C. [1958] "A statistical method for evaluating systematic relationships, *University of Kansas Suienu Bulletin* **38**, 1409–1438.

Wu, X., Jiang, C., Song, F., Li, J., Shao, Y., Xu, X. and Yan, P. [2015] "Size effect of thermal shock crack patterns in ceramics and numerical predictions," *Journal of the European Ceramic Society* **35**, 1263–1271.

Zhang, Y. L. and Ma, J. P. [2006] *Applicable Ceramic Material Manual* (Chemical Industry Press, Beijing), pp. 337–352.